

COLLECTIVE BLADE PITCH CONTROL OF FLOATING WIND TURBINES

Contents

2.1	Introduction	49
2.2	Control problem statement	51
2.3	Sliding mode control	53
2.3.1	Recalls	54
2.4	Adaptation algorithms	58
2.4.1	Adaptive super-twisting (Yuri Shtessel, Taleb, and Plestan 2012)	59
2.4.2	Simplified adaptive super-twisting (S. Gutierrez et al. 2020)	60
2.4.3	Homogeneity based controller with varying exponent parameter (Tahoumi, Plestan, et al. 2019)	65
2.5	Application to floating wind turbine	66
2.5.1	Adaptive STW controllers	66
2.5.2	Homogeneity based controller	70
2.5.3	Baseline gain scheduled PI control	70
2.6	Simulations and analysis	72
2.6.1	Scenario 1	72
2.6.2	Scenario 2	73
2.6.3	Scenario 3	76
2.7	Conclusions	81

2.1 Introduction

The main objectives of controlling a traditional onshore wind turbine in Region III are to ensure a rated production of electrical power. In order to meet these objectives, many control strategies have been proposed (Menezes Novaes, Araújo, and Bouchonneau Da Silva 2018). However, these control algorithms can not be directly applied to the floating wind turbines due to the introduction of the floating platform: the dynamics of floating platform, particularly the platform pitch motion must

be taken into consideration in order to avoid the negative damping problem (Skaare et al. 2007) that leads to instability (as detailed in General Introduction). Thus, specific control algorithms for FWT must be proposed.

Recalling the General Introduction, the main control objectives of FWT in Region III are to maintain a rated power meanwhile reducing the platform pitch motion (J. Jonkman, Butterfield, et al. 2009). Many works have been done during the last decade on this problem. Linear control based on collective blade pitch (CBP) strategy (control of the three blades pitch angles by a single control command) such as GSPI controller (J. Jonkman 2008a), linear quadratic regulator and linear parameter-varying controllers (Bagherieh and Nagamune 2015), model predictive control and feed-forward control (Schlipf, Pao, and Cheng 2012; Schlipf, Simley, et al. 2015). Most control approaches are based on linearized models of FWT (see previous chapter) that are derived from FAST software around an operating point depending especially on the wind and rotor speed. Consequently, the parameters of the controllers (that are mostly linear ones) must be tuned in different operating points to keep high performances; this tuning process has a cost and can be fastidious. A solution is the use of nonlinear control algorithms that have larger operating domains. In (Sandner et al. 2012; Schlipf, Sandner, et al. 2013; Raach et al. 2014; Homer and Nagamune 2018), nonlinear control strategies have been applied based on nonlinear models.

Due to the fact that

- the FWT system is highly nonlinear, uncertain and perturbed;
- the system modeling is not well-known and can be viewed, over a large operating domain, as a “black box”,

high order sliding mode control algorithms (Y. Shtessel et al. 2014; Cruz-Zavala and J. Moreno 2016) combined with gain/parameter adaptation laws (Yuri Shtessel, Taleb, and Plestan 2012; Tahoumi, Plestan, et al. 2019; S. Gutierrez et al. 2020) are well adapted. Such control algorithms are efficient even if the knowledge on the models is very limited and they are robust versus uncertainties and perturbations. In the sequel, the main contributions include

- the control problem statement of FWT in the Region III;
- the introduction of HOSM (super-twisting (Levant 1993) and homogeneous based control (Cruz-Zavala and J. Moreno 2016)), the gain/parameter adaptation algorithms and a new version of gain adaptation law for the super-twisting algorithm;

- the application of the adaptive HOSM solutions to the FAST nonlinear model according to different scenarios;
- the analysis and comparison of different adaptive HOSM approaches with respect to baseline GSPI control (J. Jonkman 2008a).

2.2 Control problem statement

Recalling that the FWT admits 4 operating regions (see Subsection *Operating regions* in General Introduction), this work is focused on the control problems in the Region III (also known as above-rated region). For the FWT system, the control problems in the considered region are firstly, the regulation of the power output at its rated value P_0 , preventing an overload so as to protect the electric machine and the mechanical structure. Secondly, due to the additional DOFs introduced by the floating platform, the platform motion, especially the platform pitching, must be taken into consideration in order to avoid the negative damping (Skaare et al. 2007); as conclusion, the platform pitch motion must be reduced.

In the sequel, it is supposed that the FWT is face the wind. The problem of FWT orientation control is not considered here. Then, suppose that the FWT turbine is face the wind and the generator torque is fixed at its rated Γ_{g0} ¹. So the power (P) regulation is turned into rotor speed (Ω_r) regulation according to the relation between the power, the generator torque and the rotor speed

$$P = n_g \Gamma_{g0} \Omega_r$$

where n_g the gear box ratio. Therefore, the control objectives of the FWT in Region III can be described as the following ones:

- regulation of the rotor speed Ω_r at its rated value Ω_{r0} , with $\Omega_{r0} = \frac{P_0}{n_g \Gamma_{g0}}$, P_0 being the rated power;
- reduction of the platform pitch motion, *i.e.* cancellation of the platform pitch velocity $\dot{\varphi}$.

From the reduced linearized models (1.9)-(1.11) (Section 1.3.1), the dynamics of rotor speed Ω_r and platform pitch velocity $\dot{\varphi}$ directly depend on the CBP angle β_{col} that is viewed as the control input. By this way, one concludes that the relative degree of the system with Ω_r or $\dot{\varphi}$ as output, is equal to 1. Furthermore, the two control objectives have to be achieved by a single control input; obviously,

1. In the next chapter, a generator will be supposed to equip the turbine. Then, its torque will be able to vary.

it is an under-actuated problem.

Existing solutions are, as mentioned in General Introduction, mainly based on the following ideas to solve this problem: the first solution is to use the detuned GSPI controller (Larsen and Hanson 2007; J. Jonkman 2008a) such that the natural frequency of closed-loop system is lower than the platform pitch natural frequency; this approach successfully attenuating the platform pitch motion but at a cost of larger power fluctuation. The second solution is based on modern control theory, such as LQR (Hazim Namik, Karl Stol, and J. a. Jonkman 2008; Christiansen, Knudsen, and T. Bak 2011; Christiansen, Knudsen, and T. Bak 2014) and H_∞ (Bakka and Karimi 2012; Bakka and Karimi 2012; X. Li and Gao 2015; Hara et al. 2017). The third solution is to use IBP control to increase the number of the inputs (Hazim Namik and Karl Stol 2010; H. Namik and K. Stol 2014; Lemmer, Raach, et al. 2015; Suemoto, Hara, and Konishi 2017); thus, multiple control objectives can be achieved. However, these solutions induce a great tuning effort due to the fact that the control is based on numerous linearized models, each model being obtained for an operating point. Moreover, the IBP control significantly increases the use of blade actuator comparing with the collective one, and is not completely implemented in commercial wind turbines (Menezes Novaes, Araújo, and Bouchonneau Da Silva 2018).

The solution used in this study is inspired by the work of (Lackner 2009; Lackner 2013; Cunha et al. 2014) and takes advantage from physical features of floating wind turbines. Consider that the desired rotor speed Ω_r^* is a function of platform pitch velocity

$$\Omega_r^* = \Omega_{r0} - k\dot{\varphi} \quad (2.1)$$

with k a positive constant. In this case, the desired rotor speed is no longer set at its rated value, but at a value varying with the platform pitch velocity (Lackner 2009; Lackner 2013). Such reference is based on the trade-off between rotor speed and platform pitch motion.

As shown in Figure 2.1, suppose that the platform is pitching forward/against the wind (notice that when the platform is pitching forward, $\dot{\varphi} < 0$). Then, the reference Ω_r^* is calculated higher than the rated: thanks to the control, the rotor speed increases with aerodynamic torque so as to track the reference. Meanwhile, the aerodynamic thrust captured by the rotor increases, which prevents the platform pitching forward, *i.e.* $|\dot{\varphi}|$ reduces. Thereby, according to (2.1), the rotor speed reference Ω_r^* converges to its rated value Ω_{r0} . On the contrary, when the platform is pitching downwind/with the wind, the control reduces the rotor speed since the reference rotor speed is lower than the rated one. At the same time, the aerodynamic thrust on the rotor decreases that stops the platform pitch downwind. Likewise, $|\dot{\varphi}|$ reduces and Ω_r^* converges to Ω_{r0} .

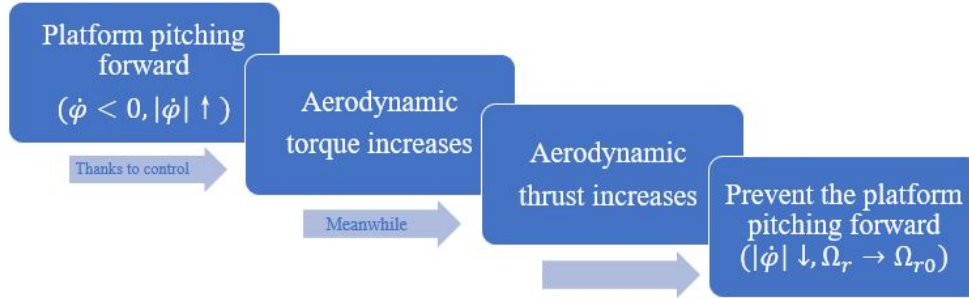


Figure 2.1 – Relationship between rotor speed and platform pitch motion under the control action.

2.3 Sliding mode control

The floating wind turbine system is a highly perturbed and uncertain nonlinear system, not only due to the elasticity of the structure (*e.g.* tower, blade, ...), but also given that the wind and waves can influence the system. Hence, the linear controllers such as GSPI (J. Jonkman 2008a; Wakui, Yoshimura, and Yokoyama 2017), LQR (Hazim Namik, Karl Stol, and J. a. Jonkman 2008; Christiansen, Knudsen, and T. Bak 2011), H_∞ (Bakka and Karimi 2012; Bakka and Karimi 2012; X. Li and Gao 2015; Hara et al. 2017) and ... are based on a linear model obtained around a given operating point; as a consequence, they have reduced operating ranges. Since the gains of linear control guarantee the expected performances only around the operating point, several sets of gains must be tuned for a set of operating points that implies a great effort of tuning.

The idea of this work is to show that nonlinear controllers with a *single* set of parameters are efficient over a large operating domain; thanks to this fact, the advantage of the proposed nonlinear control approaches is the tuning effort reduction while maintaining high level performances.

In order to develop robust nonlinear control strategies, sliding mode control (SMC) (V. Utkin 1977) is considered: it is a well-known nonlinear control strategy with properties of robustness, accuracy and finite time convergence. In fact, the standard first order SMC can be easily implemented; however, the control law of standard SMC is discontinuous. Due to the discontinuous term of the control input, chattering phenomenon (V. Utkin, Guldner, and J. Shi 1999) appears and can damage the physical components such as blade pitch actuators in this study. High order sliding mode (HOSM) (Y. Shtessel et al. 2014; Cruz-Zavala and J. Moreno 2016) control can reduce the chattering while keeping robustness and improving accuracy. Two kinds of HOSM controllers, super-twisting controller (Y. Shtessel et al. 2014) and homogeneity based (Cruz-Zavala and J. Moreno 2016) are presented in the sequel.

Furthermore, considering that system (1.9) is a simplified model with only 2 DOFs enabled, such simplified model can not describe all the characteristics of the system; the model uncertainties and the perturbations must be taken into account. As a consequence, the gains of the controllers should be sufficiently large to counteract the uncertainties/perturbations effects; it means that the gains are tuned in order to ensure high performances, *i.e.* even in the *worst* case. However, when the perturbations became relatively small, the gain is finally too large, that leads to unnecessary large variations of control (more energy consumption) and reduces the control performances. Therefore, adaptation strategies for super-twisting (through the gains) and for homogeneity based controller (through exponent parameter) are used and described respectively in the sequel.

2.3.1 Recalls

Consider the following system

$$\begin{aligned}\dot{z} &= f(z, t) + g(z, t)v \\ y &= c(z, t)\end{aligned}\tag{2.2}$$

with $z \in Z \subset \mathbb{R}^n$ the state and $v \in U \subset \mathbb{R}$ the control input. $f(z, t)$ and $g(z, t)$ are the bounded unknown nonlinear functions, and y the system output. Define the so-called sliding variable $S = S(z, t)$ such that, once $S = 0$, then $y \rightarrow 0$.

The idea of SMC is to design the control input v such that the sliding variable $S(z, t)$ is forced to reach the sliding surface $S(z, t) = 0$ in a finite time, in spite of uncertainties and perturbations. Once $S(z, t) = 0$, the system trajectories are evolving on this surface: then y goes towards 0. Notice that the sliding variable $S(z, t)$ is defined according to control objective y and the relative degree. Assume that

Assumption 1. *The relative degree ρ of system (2.2) with respect to S is constant and known with $\rho \geq 1$. Then, one gets²*

$$S^{(\rho)} = a(z, t) + b(z, t)v.\tag{2.3}$$

■

In the sequel, ρ will be equal to 1 or 2.

Assumption 2. *Functions $a(z, t)$ and $b(z, t)$ are unknown and bounded such that*

$$|a| \leq a_M, 0 < b_m \leq b \leq b_M\tag{2.4}$$

$\forall z \in Z, t > 0, a_M, b_m$ and b_M being positive constants.

■

2. In the sequel, given $k \in \mathbb{N}$, $S^{(k)}$ is the k -th time derivative of S .

Suppose that $\rho = 1$: one has

$$\begin{aligned}\dot{S} &= \underbrace{\frac{\partial S}{\partial t} + \frac{\partial S}{\partial z} f(z, t)}_{a(z, t)} + \underbrace{\frac{\partial S}{\partial z}(z, t)}_{b(z, t)} v \\ a(z, t) &= a_0(\cdot) + a_u(\cdot) \\ b(z, t) &= b_0(\cdot) + b_u(\cdot)\end{aligned}\tag{2.5}$$

with $a_0(\cdot)$ and $b_0(\cdot)$ being known functions, $a_u(\cdot)$ and $b_u(\cdot)$ being unknown and bounded uncertainties. The control objective is fulfilled by determining v such that system (2.5) is stabilized at 0 in spite of uncertainties on a and b . A solution is to define the control input v based on the standard first order sliding mode control (V. I. Utkin 1992; V. Utkin, Guldner, and J. Shi 1999) that reads as

$$v = -k \cdot \text{sign}(S)\tag{2.6}$$

with k the controller gain. Derived from Lyapunov approach (V. Utkin, Guldner, and J. Shi 1999), a first order sliding mode can be established, (*i.e.* the system trajectory converges to $S = 0$ in a finite time), if the sliding condition (with $\eta > 0$)

$$S\dot{S} \leq -\eta|S|\tag{2.7}$$

is satisfied. A sliding mode can be established if the controller gain satisfies

$$k > \frac{a_M + \eta}{b_m}\tag{2.8}$$

Then tuning of η allows to act on the convergence time t_c that is bounded by

$$t_c < \frac{S(0)}{\eta}.\tag{2.9}$$

Although the standard first order sliding mode control can achieve the control objective, the first derivative of S is discontinuous due to the discontinuity of the sign function that induces the so-called chattering phenomenon (V. Utkin, Guldner, and J. Shi 1999) that degrades the control performances. Many studies have been done in order to reduce this phenomenon, while keeping the original main characteristics (robustness, convergence in finite time). A solution is to use high order sliding mode (HOSM) algorithms (Y. Shtessel et al. 2014; Cruz-Zavala and J. Moreno 2016): the task is to keep a smoother dynamics of S by guaranteeing the high order derivatives of S equal to zero. For the r -th order sliding mode, one has (Perruquetti and Barbot 2002)

$$S = \dot{S} = \ddot{S} = \dots = S^{(r-1)} = 0.\tag{2.10}$$

Among the most popular HOSM algorithms, super-twisting (Levant 1993) and homogeneity based control are applied in this work.

Super-twisting control (Levant 1993)

The control v can be applied only for systems (2.3) with $\rho = 1$. Then, the control reads as (Levant 1993)

$$\begin{aligned} v &= -k_1 |S|^{\frac{1}{2}} \cdot \text{sign}(S) + \omega \\ \dot{\omega} &= -k_2 \cdot \text{sign}(S) \end{aligned} \quad (2.11)$$

with k_1 and k_2 the controller gains. One of the main advantage of STW is that it only depends on the sliding variable S (not on \dot{S} as most of the second order sliding mode controllers—see for example the twisting algorithm (Levant 1993)). A key point for the tuning of STW is the estimation of the minimum values of the controller gains allowing to ensure the establishment of a second order sliding mode, *i.e.*

$$S, \dot{S} \rightarrow 0 \quad (2.12)$$

From the knowledge of the bounds defined in Assumption 2, a second order sliding mode can be established in a finite time with the controller (2.11) if (Levant 1993)

$$k_1 > \frac{a_M}{b_M}, \quad k_2^2 \geq \frac{4a_M}{b_m^2} \cdot \frac{b_M}{b_m} \cdot \frac{k_1 + a_M}{k_1 - a_M} \quad (2.13)$$

In practice, the super-twisting controller ensures, in a finite time, the establishment of a "real" second order sliding mode (Levant 1993) such that

$$|S| < \mu_1 T_e^2, \quad |\dot{S}| < \mu_2 T_e \quad (2.14)$$

with T_e the control sampling time, and μ_1 and μ_2 positive constant. It is established that the sliding mode appears in a finite time with sufficiently large gains k_1 and k_2 . However, in practice, the bounds of uncertainties and perturbations are difficult to determine; furthermore, even if they are determined, they are often over-estimated that degrades the control performances. A solution is the use of adaptive gains: it allows to dynamically increase the gains when accuracy is not sufficient, and to dynamically reduce them when control objectives are reached. Such gain adaptation laws will be detailed in the sequel.

Homogeneous controller (Cruz-Zavala and J. Moreno 2016)

Another solution to establish HOSM is based on Lyapunov functions and proposed in (Cruz-Zavala and J. Moreno 2016). The control v reads as³

$$\begin{aligned} v &= -k_\rho [S_\rho]^0 \\ S_i &= [S^{(i-1)}]^{r_i} + k_{i-1}^{r_i} S_{i-1}, \quad i = 2, \dots, \rho \end{aligned} \quad (2.15)$$

with relative degree $\rho \geq 2$, $[r_1, \dots, r_\rho] = [\rho, \rho - 1, \dots, 1]$, $S_1 = S$ and (k_1, \dots, k_ρ) the controller gains. As previously, in order to ensure the establishment of a ρ^{th} -order sliding mode, the gains should fulfill the following conditions

- $\rho = 2$. The gain k_1 is arbitrarily fixed positive and k_2 is derived from

$$b_m k_2 - a_M \geq \gamma_1 k_1^2 \quad (2.16)$$

- $\rho > 2$. The gain k_1 is arbitrarily fixed positive and k_i is derived from

$$\begin{aligned} k_i &= \gamma_{i-1} k_1^{\frac{\rho}{\rho-(i-1)}}, \quad \forall i = 2, \dots, \rho - 1 \\ b_m k_\rho - a_M &\geq \gamma_{\rho-1} k_1^\rho \end{aligned} \quad (2.17)$$

with γ_{i-1} , ($i = \{2, 3, \dots, \rho - 1\}$) the parameters that are calculated to guarantee the time derivative of Lyapunov function negative definite. Table 2.1 shows the values of γ_{i-1} for $\rho = 2, 3, 4$.

Table 2.1 – Parameters γ_{i-1} (Cruz-Zavala and J. Moreno 2016).

ρ	Parameters
2	$\gamma_1 = 1.26$
3	$\gamma_2 = 1.26, \gamma_1 = 1.26$
4	$\gamma_3 = 1.26, \gamma_2 = 1.26, \gamma_1 = 1.26$

In current study the case $\rho = 2$, is under interest. One gets $r_1 = 2, r_2 = 1$

$$\begin{aligned} S_1 &= S \\ S_2 &= [\dot{S}]^2 + k_1^2 S \end{aligned} \quad (2.18)$$

and the control v reads as

$$\begin{aligned} v &= -k_2 \cdot \text{sign}(S_2) \\ &= -k_2 (|\dot{S}|^2 \text{sign}(\dot{S}) + k_1^2 S) \end{aligned} \quad (2.19)$$

Although HOSM can be established by homogeneous controller in a finite time, the controller gains of such method are also overestimated as the STW in practice, which induces high actuator energy

3. In the sequel, $[S]^n = |S|^n \text{sign}(S)$ with $n \in \mathbb{N}$.

consumption. Moreover, due to the sign function used in the control, another drawback, chattering phenomenon can appear. This phenomenon is further magnified by the overestimated gains (Obeid et al. 2018).

In the sequel, an adaptive solution of (2.15) is given by introducing a time varying exponent parameter $\bar{\alpha}$. By this way, the closed-loop accuracy can be ensured with less both chattering and energy assumption.

2.4 Adaptation algorithms

As detailed in the previous section, the choice of sufficiently large gains (versus uncertainties and perturbations) allows to guarantee the establishment of high order sliding mode. However, in many applications, the bounds of uncertainties and perturbations are difficult to determine, that is the case for FWT systems. As a consequence, the gains are often over-estimated. A solution consists to use adaptive gains or parameters with an intuitive approach: the accuracy of the closed-loop system versus the control objectives is checked and an action on the gains/parameters is made in order to guarantee a sufficient accuracy and an attenuated chattering. In this section, both such approaches are presented knowing that one of main objectives is to the limitation of the chattering.

Gain adaptation

This approach is applied to the STW controller (2.11), the controller gains k_1 and k_2 being dynamically adapted with respect to the uncertainties and perturbations. Namely, the gains are time-varying and are reduced if the accuracy is good, increased if accuracy falls (Y. Shtessel et al. 2014; Cruz-Zavala and J. Moreno 2016; Yuri Shtessel, Taleb, and Plestan 2012; S. Gutierrez et al. 2020). This way allows to reduce the amplitude of the chattering since the gains are not overestimated but adjusted to the uncertainties and perturbations. Based on this gains adaptation approach, two adaptive control laws will be used in the sequel

- the first one is the adaptive super-twisting (ASTW) control proposed by (Yuri Shtessel, Taleb, and Plestan 2012);
- the second one is the "simplified" version of adaptive super-twisting (SAST) control, that is firstly proposed in (S. Gutierrez et al. 2020).

Exponent adaptation

This approach is based on the homogeneous controller (2.15). Quite different from the previous gain adaptation, the adaptation here is achieved by introducing a parameter $\bar{\alpha}$ on the exponent terms of (2.15)

$$v = -k_\rho [S_\rho]^{\bar{\alpha}} \quad (2.20)$$

with the parameter $\bar{\alpha}$ adapted with respect to the closed loop accuracy. When the trajectory of the system is far from the origin, the controller must be robust. Then, $\bar{\alpha}$ is fixed at 0: it is equivalent to HOSM controller increasing the robustness and the accuracy of the system. When the trajectory of the system is close to the origin, a smoother linear control can be applied by varying $\bar{\alpha}$ from 0 to 1. In this case, the controller is linear that reduces the chattering effect. It finds a trade-off between accuracy and energy consumption by directly acting on terms depending on sign functions (Tahoumi, Ghanes, et al. 2018; Tahoumi, Plestan, et al. 2018b; Tahoumi, Plestan, et al. 2018a; Tahoumi, Plestan, et al. 2019). In the sequel, the parameter adaptation controller selected in this work is the homogeneity based controller with varying exponent parameter (HCVP) (Tahoumi, Plestan, et al. 2019).

2.4.1 Adaptive super-twisting (Yuri Shtessel, Taleb, and Plestan 2012)

Thanks to the adaptation law, the controller gains k_1 and k_2 in (2.11) must be dynamically adapted to the "just sufficient" values in spite of the uncertainties and perturbations. Furthermore, they must ensure the convergence of the closed-loop system and reduce the chattering effect. Recall that the control design must require no information on the bounds of uncertainties and perturbations. Following all these features, the adaptation law is defined by (Yuri Shtessel, Taleb, and Plestan 2012)

$$\dot{k}_1 = \begin{cases} \omega \sqrt{\frac{\chi}{2}} \text{sign}(|S| - \mu) & \text{if } k_1 > k_m \\ m & \text{if } k_1 < k_m \end{cases} \quad (2.21)$$

$$k_2 = \epsilon k_1$$

where k_m , ϵ , ω , χ , μ and m are positive constants, $k_1(0) > k_m$. The idea of the gain adaptation is the following

- if $|S|$ is small enough versus the accuracy defined by μ , *i.e.* $\text{sign}(|S| - \mu) < 0$, it means that the controller is efficient: the gain can be reduced. \dot{k}_1 being negative, k_1 decreases;
- if $|S|$ is larger than the desired accuracy, *i.e.* $\text{sign}(|S| - \mu) > 0$, it could be due to the fact that the gain is too small versus uncertainties and perturbations. Then, \dot{k}_1 being positive, k_1 increases;

- the parameter k_m is taken as a very small value and ensures the positiveness of k_1 .

Notice that the ASTW controller can be applied without any knowledge of $a(z, t)$ and $b(z, t)$.

2.4.2 Simplified adaptive super-twisting (S. Gutierrez et al. 2020)

As detailed in the previous section, the ASTW combines second order sliding mode algorithm and adaptive law that successfully reduces the chattering and keeps a high accuracy. Furthermore, this controller requires no information on the uncertainties and perturbation, and the adaptation law is intuitive and easily implementable. Nevertheless, the major drawback of previous algorithm is its numerous tuning parameters ($k_m, \epsilon, \omega, \chi, \mu$ and m). Furthermore, there is no tuning methodology. A first simplified adaptive super-twisting has been proposed in (S. V. Gutierrez et al. 2019) that reduced the number of tuning parameters at 2. However, the key problem with this approach is that the gains tuning process is not easy and the behaviour of the gain is not easily predictable (the adaptation law is not intuitive). Therefore, a new adaptive version of super-twisting algorithm with an intuitive adaptation law and a reduced number of parameters SAST is proposed in this work.

Assumption 3. *The relative degree ρ is equal to 1. S -dynamic reads as*

$$\dot{S} = a_0(\cdot) + b_0(\cdot)u + \varrho(z, t) \quad (2.22)$$

with $a_0(\cdot)$ and $b_0(\cdot)$ known functions, and $\varrho(z, t)$ the parametric uncertainties and external perturbations. ■

Assumption 4. *The first time derivative of the perturbation ϱ is bounded with unknown boundary δ , i.e. there exists $\delta > 0$, such that $\dot{\varrho} \leq \delta$.* ■

Consider the following state feedback u defined as

$$u = \frac{1}{b_0(\cdot)} (-a_0(\cdot) + v) \quad (2.23)$$

that linearizes the sliding variable dynamics when no perturbation/uncertainty is acting, and the “new” control input v given by

$$\begin{aligned} v &= -2L(t)|S|^{\frac{1}{2}}\text{sign}(S) + w \\ \dot{w} &= -\frac{L^2(t)}{2}\text{sign}(S) \end{aligned} \quad (2.24)$$

The controller (2.24) is based on the STW algorithm where $L(t)$ is a time-varying gain that will be tuned thanks to an adaptation law. Then, under the control (2.23)-(2.24), it follows that the

S-dynamics reads as (S. Gutierrez et al. 2020)

$$\dot{S} = -2L(t)|S|^{1/2}\text{sign}(s) + w + \varrho \quad (2.25)$$

that can be also written as

$$\begin{aligned} \dot{S} &= -2L(t)|S|^{1/2}\text{sign}(s) + \bar{w} \\ \dot{\bar{w}} &= -\frac{L^2(t)}{2}\text{sign}(s) + \dot{\varrho} \end{aligned} \quad (2.26)$$

Notice that controller (2.24) only depends on the gain $L(t)$, which simplifies its tuning. The idea now is to propose an adaptation law that dynamically changes the control gain $L(t)$ until a real second order sliding mode is established (*i.e.* (2.14) is fulfilled).

The main methodological result of the "simplified" adaptation law is formulated as following (S. Gutierrez et al. 2020)

$$\dot{L} = \begin{cases} L(|S| - \mu), & \text{if } L > L_m \\ L_m, & \text{if } L \leq L_m \end{cases} \quad (2.27)$$

where μ and L_m are positive constants, $L(0) > L_m$. The parameter L_m is introduced in order to get only positive values for $L(t)$, and can be chosen arbitrarily small. The parameter μ is tuned with respect to the desired accuracy of the closed-loop system. Notice that only two parameters are required and only the choice of μ is crucial.

Proof

Consider the STW algorithm with perturbation term

$$\begin{aligned} \dot{z}_1 &= -2L(t)z_1^{1/2}\text{sign}(z_1) + z_2 \\ \dot{z}_2 &= -\frac{L(t)^2}{2}\text{sign}(z_1) + \gamma(t, z) \end{aligned} \quad (2.28)$$

that has the same form as (2.25). Now, in order to represent system (2.28) in a convenient form for Lyapunov analysis, consider the following change of coordinates

$$\xi_1 = z_1^{1/2}\text{sign}(z_1), \quad \xi_2 = \frac{z_2}{L(t)} \quad (2.29)$$

with $L(t) > 0$. Then, from system (2.28), one gets

$$\begin{aligned}\dot{\xi}_1 &= \frac{L(t)}{2\xi_1}(-2\xi_1 + \xi_2) \\ \dot{\xi}_2 &= \frac{L(t)}{2\xi_1} \left(-\xi_1 + \frac{2\xi_1\gamma(t, \xi)}{L^2(t)} \right) - \frac{\dot{L}(t)}{L(t)}\xi_2\end{aligned}\quad (2.30)$$

Then, the system (2.30) can be rewritten as

$$\dot{\xi} = \frac{L}{2\xi_1} \left\{ (\mathbf{A} - \mathbf{S}_\infty^{-1}\mathbf{C}^T\mathbf{C})\xi + \frac{1}{L^2}\mathbf{D} \right\} - \frac{\dot{L}(t)}{L(t)}\mathbf{B}\mathbf{B}^T\xi \quad (2.31)$$

with

$$\begin{aligned}\xi &= \begin{bmatrix} \xi_1 \\ \xi_2 \end{bmatrix}, \quad \mathbf{A} = \begin{bmatrix} 0 & 1 \\ 0 & 0 \end{bmatrix}, \quad \mathbf{B} = \begin{bmatrix} 0 \\ 1 \end{bmatrix} \quad \mathbf{C} = \begin{bmatrix} 1, & 0 \end{bmatrix}, \\ \mathbf{S}_\infty &= \begin{bmatrix} 2 & 1 \\ 1 & 0 \end{bmatrix}, \quad \mathbf{D}(t, \xi) = \begin{bmatrix} 0 \\ 2\xi_1\gamma(t) \end{bmatrix}\end{aligned}$$

with \mathbf{S}_∞ a symmetric and positive definite matrix solution of the algebraic Lyapunov equation $\mathbf{S}_\infty + \mathbf{A}^T\mathbf{S}_\infty + \mathbf{S}_\infty\mathbf{A} - \mathbf{C}^T\mathbf{C} = 0$. Consider the following Lyapunov candidate function

$$V_{(\xi, L)} = V_{(\xi)} + \frac{1}{2}(L(t) - L^*)^2 \quad (2.32)$$

with $V_{(\xi)} = \xi^T\mathbf{S}_\infty\xi$. Taking the time derivative of Lyapunov function along the trajectories of the system (2.31), it follows that

$$\begin{aligned}\dot{V}_{(\xi, L)} &= \frac{1}{2\xi_1} \left[-L(t)\xi^T\mathbf{S}_\infty\xi - L(t)\xi^T\mathbf{C}^T\mathbf{C}\xi + 2\xi^T\mathbf{S}_\infty\mathbf{D} \right] \\ &\quad + \dot{L}(t) \left[(L(t) - L^*) - \frac{2}{L(t)}\xi^T\mathbf{B}\mathbf{B}^T\xi \right]\end{aligned}\quad (2.33)$$

The function $V_{(\xi)}$ satisfies the following inequalities

$$\lambda_{min}(\mathbf{S}_\infty)\|\xi\|^2 \leq V_{(\xi)} \leq \lambda_{max}(\mathbf{S}_\infty)\|\xi\|^2 \quad (2.34)$$

where $\lambda_{min}(\mathbf{S}_\infty)$ and $\lambda_{max}(\mathbf{S}_\infty)$ are the minimum and maximum eigenvalues of the matrix \mathbf{S}_∞ respectively; one gets

$$\xi_1 \leq \xi \leq \frac{V_{(\xi)}^{1/2}}{\lambda_{min}^{1/2}(\mathbf{S}_\infty)} \quad (2.35)$$

Consider the norm of the nonlinear term $2\xi^T\mathbf{S}_\infty\mathbf{D}$, and transformed the perturbation satisfies

$\mathbf{D}(t, \xi) \leq \delta \xi$ (J. A. Moreno 2009). Taking into account (2.33) and (2.34), one obtains

$$\begin{aligned} \dot{V}_{(\xi, L)} &\leq \frac{1}{2\xi_1} \left[-L(t)V_{(\xi)} + 2\mathbf{S}_\infty \delta \xi^2 - L(t)\xi^T \mathbf{C}^T \mathbf{C} \xi \right] \\ &\quad + \dot{L}(t) \left[(L(t) - L^*) - \frac{2}{L(t)} \xi^T \mathbf{B} \mathbf{B}^T \xi \right] \\ \dot{V}_{(\xi, L)} &\leq -\eta V_{(\xi)}^{1/2} - \frac{L(t)}{2} \xi_1 \\ &\quad + \dot{L}(t) \left[(L(t) - L^*) - \frac{2}{L(t)} \xi^T \mathbf{B} \mathbf{B}^T \xi \right] \end{aligned} \quad (2.36)$$

with

$$\eta = \frac{L(t) - q}{2\lambda_{\min}^{-1/2}(\mathbf{S}_\infty)}, \quad q = \frac{2\delta \mathbf{S}_\infty}{\lambda_{\min}(\mathbf{S}_\infty)}$$

By adding and subtracting the term $\kappa L(t) - L^*$ in (2.36), one obtains

$$\begin{aligned} \dot{V}_{(\xi, L)} &\leq -\eta V_{(\xi)}^{1/2} - \frac{L(t)}{2} \xi_1 - \kappa L(t) - L^* + \kappa L(t) - L^* \\ &\quad + \dot{L}(t) \left[(L(t) - L^*) - \frac{2}{L(t)} \xi^T \mathbf{B} \mathbf{B}^T \xi \right] \end{aligned} \quad (2.37)$$

Using Jensen's inequality

$$(a^q + b^q)^{1/q} \leq a + b, \quad q > 0$$

and choosing $a = V_{(\xi)}$, $b = (L(t) - L^*)^2$ and $q = \frac{1}{2}$, then one has

$$-\eta V_{(\xi)}^{1/2} - \kappa L(t) - L^* \leq -\iota V_{(\xi, L)}^{1/2} \quad (2.38)$$

with $\iota = \min(\eta, \kappa)$. Taking into account (2.38), and assuming there exist positive constant L^* such that $L(t) - L^* < 0 \forall t \geq 0$. In view of the above assumption, equation (2.37) can be reduced to the following

$$\dot{V}_{(\xi, L)} \leq -\iota V_{(\xi, L)}^{1/2} + \epsilon \quad (2.39)$$

with

$$\epsilon = -\frac{L(t)}{2} \xi_1 - L(t) - L^* (\dot{L}(t) - \kappa) - \frac{2\dot{L}(t)}{L(t)} \xi^T \mathbf{B} \mathbf{B}^T \xi$$

Next, through the study of ϵ and its sign, stability of the closed-loop system is analyzed. More precisely, the behavior of the time derivative of the Lyapunov function is analyzed. To ensure the stability of $\dot{V}_{(\xi, L)}$, consider the following cases.

Case 1. Suppose that $L(t) > L_m$, and $|S| - \mu > 0$. Then, $L(t)$ is increased until the second order slid-

ing mode is established. If $\kappa < L(t)(|S| - \mu)$, Then, ϵ is negative, and it follows that $\dot{V}_{(\xi,L)} \leq -\iota V_{(\xi)}^{1/2}$ with $\iota = \min(\eta, \kappa)$.

Case 2. Suppose now $L(t) \leq L_m$ that implies $\dot{L}(t) = L_m$, and

$$\epsilon = -\frac{L(t)}{2}\xi_1 - L(t) - L^*(L_m - \kappa) - \frac{2L_m}{L(t)}\xi^T \mathbf{B}\mathbf{B}^T \xi \quad (2.40)$$

In this case, considering $\kappa = L_m$, which yields $\epsilon \leq 0$, then, the 2-sliding mode is established, one gets

$$\dot{V}_{(\xi,L)} \leq -\iota V_{(\xi,L)}^{1/2} \quad (2.41)$$

As soon as inequality (2.41) is fulfilled in finite-time, the SAST control law (2.27) drives the sliding variable S and its derivative to zero in finite time, that is estimated as

$$t_c \leq \frac{2V_{(\xi,L)}^{1/2}(0)}{\iota} \quad (2.42)$$

Thus, the states ξ_1 and ξ_2 converge to zero in finite-time. This implies that also the states z_1, z_2 will converge to zero in finite-time.

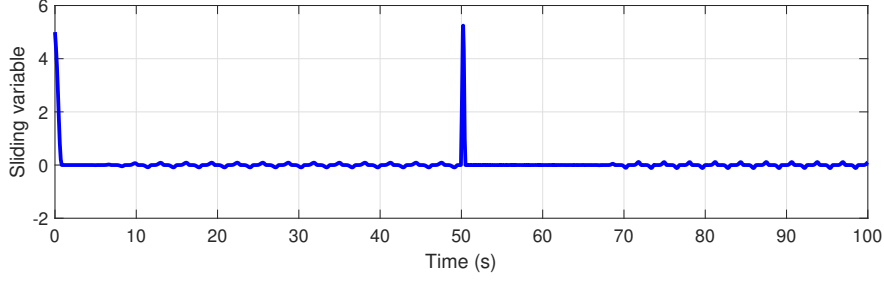
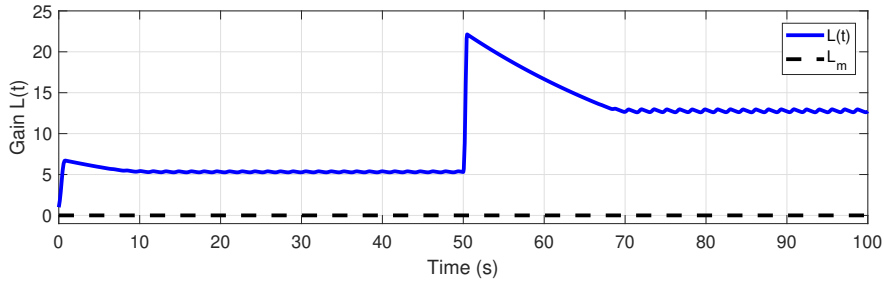
Case 3. Suppose that $L(t) > L_m$, and $|S| - \mu < 0$, that implies $L(t)$ is reducing in accordance with (2.27), then, the term ϵ becomes positive. Hence, in view of (2.39), $\dot{V}_{(\xi,L)}$ becomes sign indefinite. As soon as the state $|S|$ becomes greater than μ (this happens in finite time), the condition that defines Case 1 holds, i.e. it means that $L(t)$ shall increase in accordance with (2.27) that guarantee $\dot{V}_{(\xi,L)}$ is negative definite.

Academic example

Consider the uncertain system $\dot{S} = u + \varrho(t)$ with $\varrho(t)$ defined as

$$\varrho(t) = \begin{cases} 10 \sin(2t) & \text{if } t \leq 50 \text{ sec} \\ 50 \cos(2t) & \text{if } t > 50 \text{ sec} \end{cases}$$

The initial value of the sliding variable is defined as $S(0) = 5$. The control input u is defined as (2.23)-(2.24)-(2.27) with $a_0 = 0$ and $b_0 = 1$. Parameters of the controller have been tuned in order to get good behaviour and performances, *i.e.* $L_m = 0.005$, $\mu = 0.03$. Figure 2.2 displays the sliding variable $S(t)$. The efficiency of the proposed adaptation algorithm is described in Figure 2.3: the gain $L(t)$ increases until a sliding mode is established. Thus, the gain starts reducing. This gain reduction is reversed as soon as the sliding variable starts deviating from the vicinity of $S = 0$.

Figure 2.2 – Sliding variable $S(t)$ versus time (sec).Figure 2.3 – Adaptive gain $L(t)$ versus time (sec).

2.4.3 Homogeneity based controller with varying exponent parameter (Tahoumi, Plestan, et al. 2019)

The approach has been very recently proposed by (Tahoumi, Plestan, et al. 2019) and is based on the homogeneous controller (2.15). The adaptation law is made by introducing a time varying exponent parameter $\bar{\alpha}$ such that the control law now reads as

$$v = -k_\rho [S_\rho]^{\bar{\alpha}} \quad (2.43)$$

with k_ρ , S_ρ tuned as (2.15) and $\bar{\alpha} \in [0, 1]$ with the adaptive law

$$\bar{\alpha} = \max\left(-\bar{\beta} \sum_{i=1}^{\rho} \frac{|S^{(i-1)}|}{|S^{(i-1)}| + \epsilon_{S_i}} + 1, 0\right) \quad (2.44)$$

with ϵ_{S_i} a positive constant and $\bar{\beta} > 1$ tuned by the user. The idea of the adaptation is the following

- if $|S|$ and its time derivatives are small enough, the exponent term $\bar{\alpha}$ is forced towards 1. Formally, if a high order sliding mode is established, one gets $\bar{\alpha} = 1$: a linear controller versus S_ρ is obtained

$$v = -k_\rho S_\rho \quad (2.45)$$

that reduces the energy consumption;

- on the contrary, if a sliding mode is not established, $\bar{\alpha}$ reaches 0 and increases the control accuracy given that the control law appears as a sliding mode one versus S_ρ

$$v = -k_\rho \text{sign}(S_\rho) \quad (2.46)$$

- ϵ_{S_i} and $\bar{\beta}$ are the $\rho + 1$ parameters acting on the accuracy of the controller.

In conclusion, this approach allows to get a trade-off between accuracy and energy consumption.

2.5 Application to floating wind turbine

As described in Section 2.2, the control input u and the output y can be defined as (β_{col} being the collective blade pitch angle, and Ω_r (resp. Ω_r^*) being the rotor (resp. reference) velocity)

$$\begin{aligned} u &= \beta_{col} \\ y &= \Omega_r - \Omega_r^* \end{aligned} \quad (2.47)$$

with Ω_r^* defined by (2.1). The control objective is to ensure y converging to 0. System (1.10)-(1.11) with the output y has a relative degree with respect to the CBP angle β_{col} equal to 1. Consequently, the sliding variable vector S is defined as

$$S = \Omega_r - \Omega_{r0} + k\dot{\varphi} \quad (2.48)$$

Then, the time derivative of S reads as

$$\dot{S} = a(\cdot) + b(\cdot)u \quad (2.49)$$

with $a(\cdot)$ and $b(\cdot)$ unknown but bounded functions, derived from uncertain functions $f_{wt}(x, t)$ and $-g_{wt}(x, t)$ ⁴ (see system (1.13) detailed in Chapter 1).

2.5.1 Adaptive STW controllers

Given that the control strategies applied in the sequel are based on STW algorithm, system on which they are applied must have a relative degree equals to 1. With S defined as (2.48), that is in the case.

4. Notice that the term $b(\cdot)$ must be positive according to Assumption 2, but the term $g_{wt}(x, t)$ is negative according to the linearized model. Thus, define that $b(\cdot) = -g_{wt}(x, t)$.

ASTW based control law

Recall that the ASWT algorithm can be applied without the knowledge of $a(\cdot)$ and $b(\cdot)$. Therefore, the control input reads as

$$\begin{aligned}
 u &= -k_1 |S|^{\frac{1}{2}} \text{sign}(S) - \int_0^t k_2 \text{sign}(S) d\tau \\
 \dot{k}_1 &= \begin{cases} \omega \sqrt{\frac{\chi}{2}} \text{sign}(|S| - \mu) & \text{if } k_1 > k_m \\ m & \text{if } k_1 < k_m \end{cases} \\
 k_2 &= \epsilon k_1
 \end{aligned} \tag{2.50}$$

SAST based control law

As mentioned in Subsection 2.4.2, the formal proof of SAST algorithm has been made based on the Assumption 3, with $a_0(\cdot)$ and $b_0(\cdot)$ supposed to be well-know terms. can be derived from system model. Recalling that, for a given wind speed V and a given rotor speed Ω_r , the wind turbine model can be written as a linear one, it is possible to numerically evaluate the terms $a(x, t)$ and $b(t)$ from FAST software. Indeed, for each couple wind speed-rotor speed, from the linearized model (1.9) around this operating point, $a(x, t)$ and $b(t)$ are derived from system metrics $A_{Avg}(x, t)$, $B_{Avg}(x, t)$ and the state vector x . Figure 2.4 displays the evolution of $b(t)$ with respect to the rotor speed Ω and the wind speed V . Consider that $b(t)$ can be written as

$$b(t) = b_0 + b_u(t)$$

with b_0 being the nominal term and $b_u(t)$ describing the uncertainties on $b(t)$. From Figure 2.4, $b(t)$ is bounded between 0.2282 and 1.2603 on the operating domain. Furthermore, one can arbitrarily state $b_0 = 0.7403$ that gives $-0.5121 \leq b_u(t) \leq 0.5200$. Thus, $|b_u(t)| < b_0$.

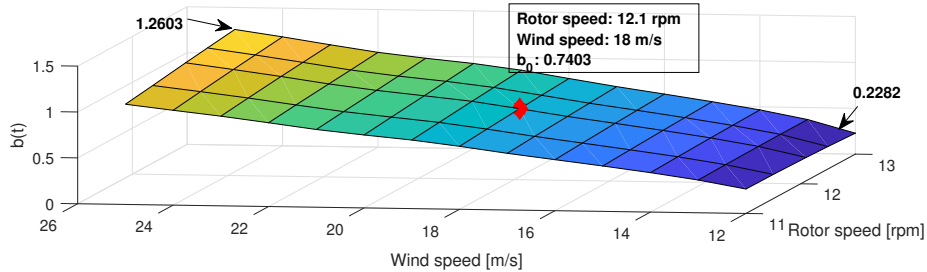


Figure 2.4 – Function $b(t)$ versus rotor speed Ω (rpm) and wind speed V (m/s).

Consider now that $a(x, t)$ can be written as

$$a(x, t) = \underbrace{(a_0 + a_u(t))}_{h(t)} \cdot x \quad (2.51)$$

with a_0 1×3 -vector the nominal term and $a_u(t)$ 1×3 -vector containing the uncertainties on $a(x, t)$ that is varying with the considered operating points. Denote $h(t) = [h_1 \ h_2 \ h_3] = a_0 + a_u(t) = [a_{10} \ a_{20} \ a_{30}] + [a_{1u}(t) \ a_{2u}(t) \ a_{3u}(t)]$. By a similar way than previously, Figure 2.5 displays the evolution of each component of $h(t)$ with respect to the rotor speed Ω_r and the wind speed V . From this figure, one can find that $h(t)$ is bounded in the operating domain, and thereby, $a(x, t)$ is bounded as well. Furthermore, considering $h(t)$ at the rated rotor speed and the rated wind speed, one can arbitrarily state $a_0 = [a_{10} \ a_{20} \ a_{30}] = [-0.1753 \ -1.7760 \ -0.1487]$.

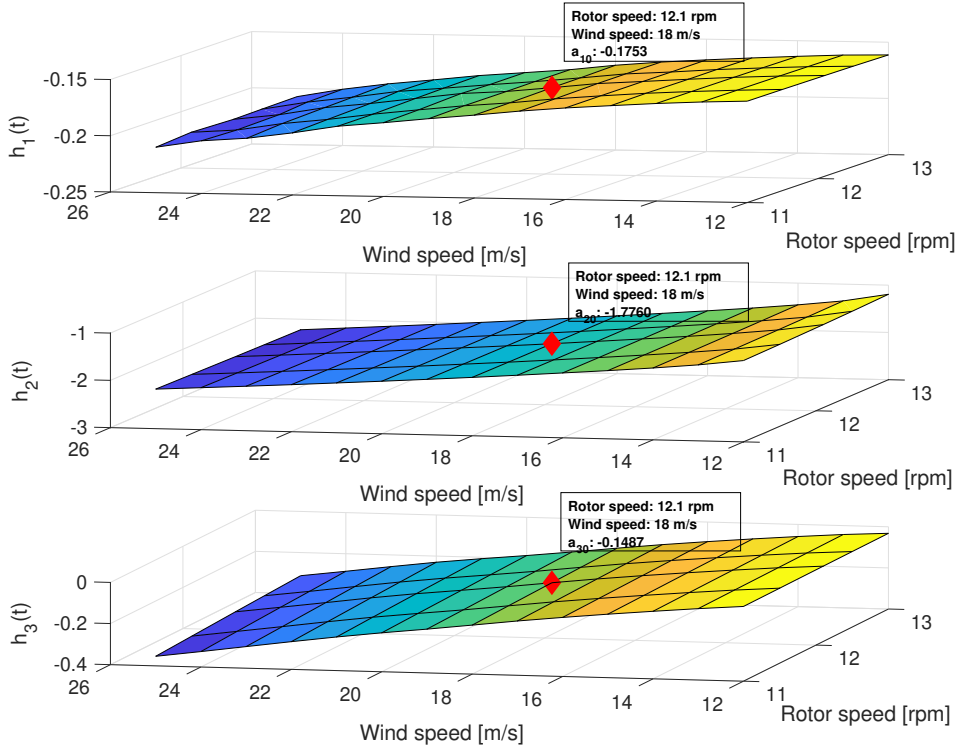


Figure 2.5 – Vector $h(t)$ versus rotor speed Ω (rpm) and wind speed V (m/s).

Then, from (2.49), one gets

$$\dot{S} = [a_0 + a_u(t)] \cdot x + [b_0 + b_u(t)]u \quad (2.52)$$

Considering the control law as (2.23)

$$u = \frac{v - a_0 \cdot x}{b_0}, \quad (2.53)$$

one gets

$$\dot{S} = v + \underbrace{\left(a_u - \frac{b_u}{b_0} a_0\right) \cdot x + \frac{b_u}{b_0} \cdot v}_{\varrho} \quad (2.54)$$

Recalling that $|b_u(t)| < |b_0|$, it is trivial to show that the control v as defined as (2.24)

$$\begin{aligned} v &= -2L|S|^{\frac{1}{2}}\text{sign}(S) - \int_0^t \frac{L^2}{2}\text{sign}(S)d\tau \\ \dot{L} &= \begin{cases} L(|S| - \mu), & \text{if } L > L_m \\ L_m & \text{if } L \leq L_m \end{cases} \end{aligned} \quad (2.55)$$

allows the establishment of a second order sliding mode. However, given that all the other controllers are designed without prefeedback (2.23)⁵, SAST will be used in the similar way, *i.e.*

$$u = -2L|S|^{\frac{1}{2}}\text{sign}(S) - \int_0^t \frac{L^2}{2}\text{sign}(S)d\tau \quad (2.56)$$

Indeed, considering S -dynamics

$$\dot{S} = [a_0 + a_u(t)] \cdot x + [b_0 + b_u(t)]u \quad (2.57)$$

one gets

$$\dot{S} = \{[a_0 + a_u(t)] \cdot x + b_u(t) \cdot u\} + b_0 \cdot u \quad (2.58)$$

then,

$$\dot{S} = \underbrace{[a_0 + a_u(t)] \cdot x + [b_u(t) - 1 + b_0] \cdot u}_{\varrho} + u \quad (2.59)$$

Recalling that $b_0 = 0.7403$ and $-0.5121 \leq b_u(t) \leq 0.5200$, one gets

$$-0.7718 \leq b_u(t) - 1 + b_0 \leq 0.2603$$

it means that the control input u can always act on S -dynamics, in spite of the fact that ϱ depends on u . Then, the system (2.59) is under the form of (2.22). SAST algorithm can be directly applied.

5. Indeed, the objective is to have the most simple control structure.

2.5.2 Homogeneity based controller

As detailed in Subsection 2.3.1, the homogeneity based controller can be applied only if the relative degree ρ is larger or equal to 2. However, as shown in (2.49), the relative degree is equal to 1. A solution consists in acting through the time derivative of u . Denoting $\bar{u} = \dot{u}$, one has

$$\ddot{S} = \bar{a}(\cdot) + \bar{b}(\cdot)\bar{u} \quad (2.60)$$

with $\bar{a}(\cdot)$ and $\bar{b}(\cdot)$ respectively derived from $a(\cdot)$ and $b(\cdot)$. Then, considering (2.60), the relative degree ρ equals to 2 with respect to the *new* input \bar{u} . In this case, the HCVP control algorithm can be applied and reads as

$$\begin{aligned} \bar{u} &= -k_2[S_2]^{\bar{\alpha}} \\ \bar{\alpha} &= \max\left(-\bar{\beta} \sum_{i=1}^2 \frac{|S^{(i-1)}|}{|S^{(i-1)}| + \epsilon_{S_i}} + 1, 0\right) \end{aligned} \quad (2.61)$$

with $S_2 = [\dot{S}]^2 + k_1^2 S$ and $S_1 = S$.

2.5.3 Baseline gain scheduled PI control

The gain-scheduled proportional integral (GSPI) controller based on the CBP control developed by (J. Jonkman, Butterfield, et al. 2009) is a well-known controller for the FWT in Region III. It is widely used as the baseline controller by the community of researchers to compare the performances of the proposed controllers. The GSPI control is given by

$$\beta_{col} = K_p e(t) + K_i \int_0^t e(\tau) d\tau \quad (2.62)$$

with

- $e(t)$ the error between the actual generator speed Ω_g and the rated generator speed Ω_{g0}

$$e(t) = \Omega_g - \Omega_{g0} = n_g(\Omega_r - \Omega_{r0}) \quad (2.63)$$

- K_p and K_i the proportional and integral gain respectively, which are given by

$$K_p = \frac{2I_D \Omega_{r0} \xi \omega_n}{n_g \left(-\frac{\delta P}{\delta \beta_{col}} \right)} \quad (2.64)$$

and

$$K_i = \frac{I_D \Omega_{r0} \omega_n^2}{n_g \left(-\frac{\delta P}{\delta \beta_{col}} \right)} \quad (2.65)$$

with I_D the drive train inertia of the low-speed shaft, ξ and ω_n the closed-loop natural frequency and damping ratio respectively. The term $\delta P / \delta \beta_{col}$ is the sensitivity of the rotor aerodynamic power to collective blade pitch angle that depends on the wind speed, rotor speed and blade pitch angle; its value can be calculated by FAST linearization program and varies for different operating points, as shown in Table 2.2. Therefore, the controllers gains K_p and K_i are viewed as functions of the collective blade pitch angle. Detailed information of the power sensitivity and controller gains can be found in (J. Jonkman, Butterfield, et al. 2009).

Table 2.2 – Sensitivity $\delta P / \delta \beta_{col}$ versus wind speed, rotor speed and blade pitch angle (J. Jonkman, Butterfield, et al. 2009).

Wind speed (m/s)	Rotor speed (rpm)	Blade pitch angle (°)	$\delta P / \delta \beta_{col}$ (watt/rad)
11.4 (Rated)	12.1	0.00	-28.24E+6
12	12.1	3.83	-43.73E+6
13	12.1	6.60	-51.66E+6
14	12.1	8.70	-58.44E+6
15	12.1	10.45	-64.44E+6
16	12.1	12.06	-70.46E+6
17	12.1	13.54	-76.53E+6
18	12.1	14.92	-83.94E+6
19	12.1	16.23	-90.67E+6
20	12.1	17.47	-94.71E+6
21	12.1	18.70	-99.04E+6
22	12.1	19.94	-105.90E+6
23	12.1	21.18	-114.30E+6
24	12.1	22.35	-120.20E+6
25	12.1	23.47	-125.30E+6

Equation (2.62) shows that the GSPI control regulates only the rotor speed to its rated value by actuating the collective blade pitch angle. Considering the negative damping problem introduced by the floating structure, a solution is to ensure the smallest closed-loop natural frequency lower than the smallest system natural frequency (*i.e.* the natural frequency of floating structure) (J. Jonkman

2008a; Larsen and Hanson 2007).

As conclusion, the gains K_p and K_i are reevaluated at each operating point depending on wind speed, rotor speed and blade pitch angle. From (J. Jonkman, Butterfield, et al. 2009), by applying such approach, the controller can achieve the control objectives in Region III.

2.6 Simulations and analysis

In this section, simulations are made by co-simulation between FAST and Matlab/Simulink. As detailed in Section 1.4, the model used is the NREL 5MW OC3-Hywind FWT one. All simulations have been made over 600 seconds. The integration algorithm is ODE1 (Euler) with a fixed step equal to 0.0125 *sec*. Considering the real applications, blade pitch angles are saturated as $[0^\circ, 90^\circ]$ whereas the blade pitch rates limit is $8^\circ/s$ (J. Jonkman, Butterfield, et al. 2009). Three scenarios of simulations are made in the sequel in order to evaluate the performances of the proposed adaptive controllers.

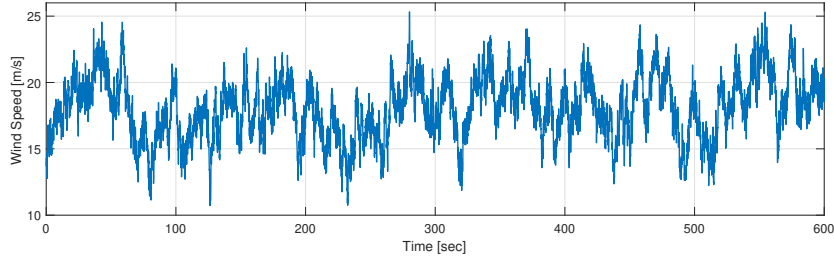
- **Scenario 1** is considered to evaluate the efficiency of the proposed SAST controller. Being a new adaptive control algorithm, SAST controller is firstly evaluated on a reduced FAST nonlinear model with only wind disturbance, without wave. Moreover, the performances of SAST are compared with the ASTW control;
- **Scenario 2** is made in order to check that the proposed control algorithms are working well on the full DOFs FAST nonlinear model. Namely, with a single set of parameters, the controller gains are adapted in different ranges of wind speed. For sake of simplicity, only ASTW controller is checked, and the performances are compared to GSPI control;
- **Scenario 3** evaluates all the three controllers (ASTW, SAST and HCVP) in more or less realistic conditions. The full DOFs FAST nonlinear model is used whereas wind speed varies in Region III with irregular waves. The performances are compared to GSPI control.

The parameter k of sliding variable (2.48) is equal to 16.7 in all the three scenarios.

2.6.1 Scenario 1

This scenario focuses on the evaluation of SAST controller in a “simple case” described as follows: only 2DOFs are enabled (rotor speed and platform pitch) in the FAST code, 18*m/s* stochastic wind with 15% turbulence intensity (see Figure 2.6); still water.

The ASTW and SAST controllers have been tuned as depicted in Table 2.3. Notice the difference

Figure 2.6 – **Scenario 1**. Wind speed (m/s) versus time (sec).

of parameters number. The parameters have been tuned in order to get the best results for each controller.

Table 2.3 – **Scenario 1**. Controller parameters.

ASTW	$\omega = 0.001, \chi = 2, \epsilon = 0.05, k_m = 0.0001, \mu = 0.01, \eta = k_m$
SAST	$L_m = 0.0001, \mu = 0.02$

The simulation results are displayed in Figure 2.7 and show comparison with GSPI. Obviously, the SAST control successfully achieves both the control objectives, *i.e.* regulation of the rotor speed around its rated value, and reduction of the platform pitch rate. Table 2.4 shows that the SAST algorithm allows better performances than GSPI controller; comparing with ASTW, SAST has similar performances but the advantage is its reduced number of parameters (see Table 2.3). Since only 2 DOFs are enabled, the rest of DOFs are considered rigid; therefore, the platform roll, yaw and fatigue life of the wind turbine components are not evaluated in this scenario. All of those performance indicators will be evaluated and compared in a more realistic condition in Scenario 3.

Table 2.4 – **Scenario 1**. RMS values of rotor speed error and platform pitch rate with SAST, ASTW and GSPI controllers

RMS	Rotor speed error (rpm)	Platform pitch rate (deg/s)
SAST	0.4954	0.0685
ASTW	0.4943	0.0603
GSPI	1.2540	0.0730

2.6.2 Scenario 2

For this scenario, only the ASTW and GSPI controllers are applied on the full-DOFs enabled FAST nonlinear model. The controllers performances are compared under irregular wave with significant height of 3.25 m and peak spectral period of 9.7 s , with 3 cases of wind conditions (see Figure 2.8)

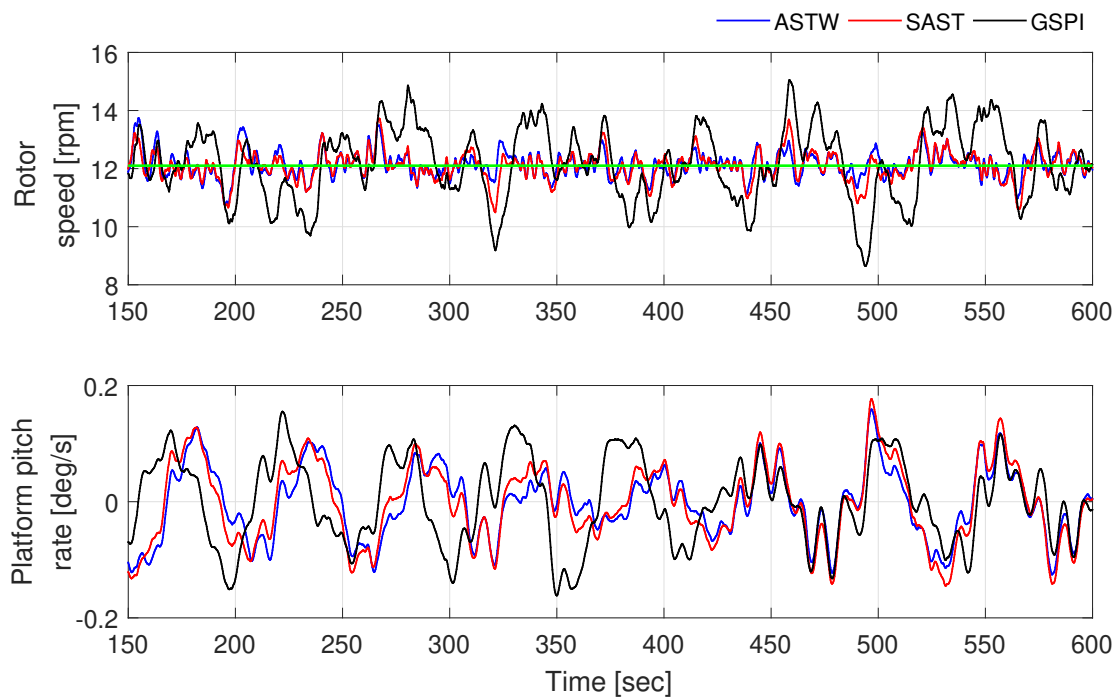


Figure 2.7 – **Scenario 1. Top.** Rotor speed Ω_r (*rpm*) versus time (*sec*). The green line is the rated value of rotor speed that is the control objective. **Bottom.** Platform pitch rate $\dot{\varphi}$ (*deg/s*) versus time (*sec*).

- Case 1: 16 m/s stochastic wind, 5% turbulence intensity;
- Case 2: 18 m/s stochastic wind, 5% turbulence intensity;
- Case 3: 20 m/s stochastic wind, 5% turbulence intensity.

A single set of parameters is used for ASTW controller in the 3 cases ($\omega = 0.001$, $\chi = 2$, $\epsilon = 0.05$, $k_m = 0.12$, $\mu = 0.01$ and $\eta = k_m$). The purpose of this scenario is to illustrate the efficiency of adaptive law on the full DOFs FAST nonlinear model, even if only a single set of parameter is used.

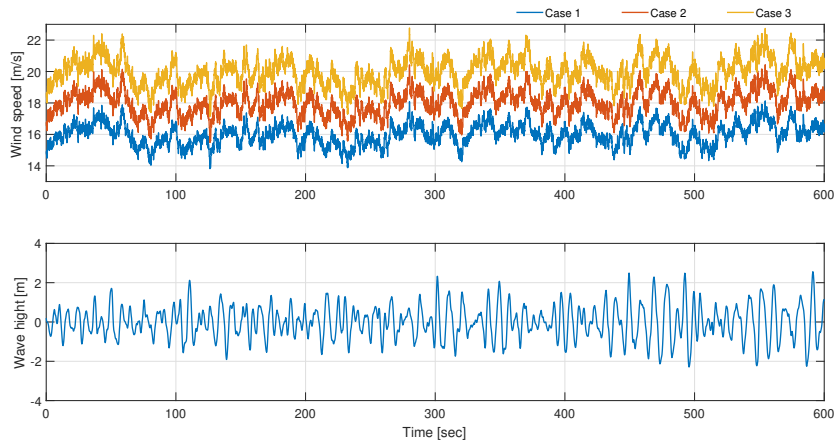


Figure 2.8 – **Scenario 2. Top.** Wind speed (m/s) versus time (sec). **Bottom.** Wave height (m) versus time (sec).

Figure 2.9 shows the main normalized performance indicators: root mean square (RMS) of rotor speed error, RMS of power error, RMS of platform pitch rate and variation (VAR) of blade pitch angle. ASTW and GSPI allow to obtain very similar performances (through RMS) concerning the rotor speed/power error in the 3 cases. Concerning the platform pitch rate, the ASTW gives smaller RMS values than GSPI; namely, the platform pitch motion is reduced with respect to GSPI. Recall that such performances are carried out with only one set of parameters while the GSPI needs more parameters (see Table 2.2). A drawback of ASTW controller is that it stimulates more the blade pitch angle actuator (see VAR of blade pitch angle in Figure 2.9). Finally, recall that Scenario 2 considers only 5% wind turbulence; Scenario 3 will propose more realistic and different conditions.

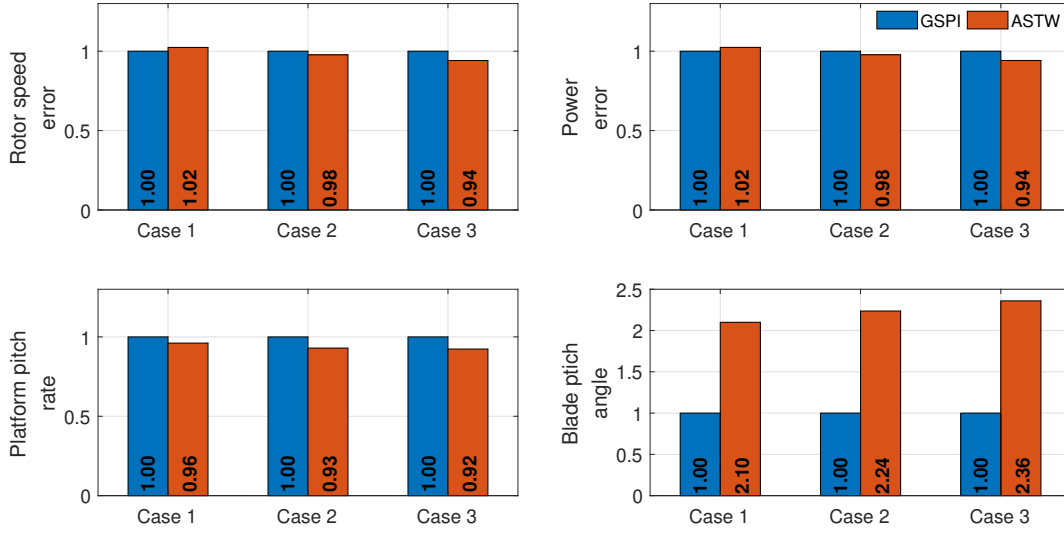


Figure 2.9 – **Scenario 2.** Normalized performance indicators for the 3 cases. **Top-left.** RMS of rotor speed error. **Top-right.** RMS of power error. **Bottom-left.** RMS of platform pitch rate. **Bottom-right.** VAR of blade pitch angle.

2.6.3 Scenario 3

It has been shown in the previous scenarios that

- the proposed SAST control is efficient for the FWT control application on the reduced FAST nonlinear model and has good performances with respect to perturbations and uncertainties of the system.
- the ASTW controller is working well considering the full DOFs FAST nonlinear model, in different wind conditions with reduced turbulence with only a single phase of tuning;

In the Scenario 3, conditions are more close from real ones and are described as

- all-DOFs enabled FAST nonlinear model;
- 18 m/s stochastic wind with 15% turbulence intensity (Figure 2.6);
- irregular wave with significant height of 3.25 m and peak spectral period of 9.7 s (Figure 2.8-bottom).

The three adaptive controllers (ASTW, SAST and HCVP) are now applied and compared with GSPI. The controller parameters are given in Table. 2.5.

Table 2.5 – **Scenario 3**: controller parameters.

ASTW	$\omega = 0.001, \chi = 2, \epsilon = 0.03, \mu = 0.05, \eta = k_m$
SAST	$L_m = 0.0001, \mu = 0.06$
HCVP	$\epsilon_{S_1} = 0.05, \epsilon_{S_2} = 0.02, k_1 = 0.11, k_2 = 0.015, \bar{\beta} = 1.2$

Figure 2.10 shows the main variables of the FWT obtained by the four controllers: the power, the rotor speed, the platform pitch rate and the blade pitch angle. Clearly, all the controllers allow to achieve the control objectives recalling that the controllers are designed on a 2 DOFs system, and applied to the full DOFs nonlinear model. The generator power and the rotor speed are varying around their rated values, *i.e.* 5 MW and 12.1 rpm respectively. The platform pitch rate is varying around 0 meaning that the platform pitch motion is limited and the system is stabilized.

For a sake of clearly, the performance indicators are normalized with respect to GSPI (see Figures 2.11, 2.12 and 2.13). As a consequence, a value smaller/larger than 1 means that the performance of the control is better/worse than GSPI. All the performance indices are computed between 150 sec and 600 sec in order to reduce the influence of the initial condition.

From Figure 2.11-top. the adaptive controllers (ASTW, SAST and HCVP) have smaller RMS for rotor speed/power error and platform pitch rate than GSPI; it means that both the two control objectives are achieved with better performances than GSPI. Of course, such improvements have a cost and lead to a larger value of the VAR of blade pitch angle: the adaptive controllers are using by a more intensive way, the blade pitch actuator. However, since the blade pitch angle saturation ($[0^\circ, 90^\circ]$) and rate limiter ($8^\circ/\text{s}$ maximum) are taken into consideration in the simulations, the controllers can be applied in practice. Furthermore, Figure 2.11-bottom displays the RMS of the platform rotations (yaw, pitch and roll angle) and their rates. Although those indicators are not so important than the previous ones, they should be kept as low as possible in order to get a lower tower base bending load. All these indicators are smaller with adaptive controllers than with GSPI. These controllers improve the associated performances. Furthermore, notice that the three adaptive controllers greatly reduce the roll and the roll rate comparing with GSPI.

Fatigue damage equivalent load (DEL) is used to measure the fatigue load of structure (as detailed in Section 1.4.3) is evaluated for the tower base (TB), the blade root (BR) (see Figure 2.12) and the mooring lines (see Figure 2.13). Figure 2.12 shows DEL performances of the proposed controllers

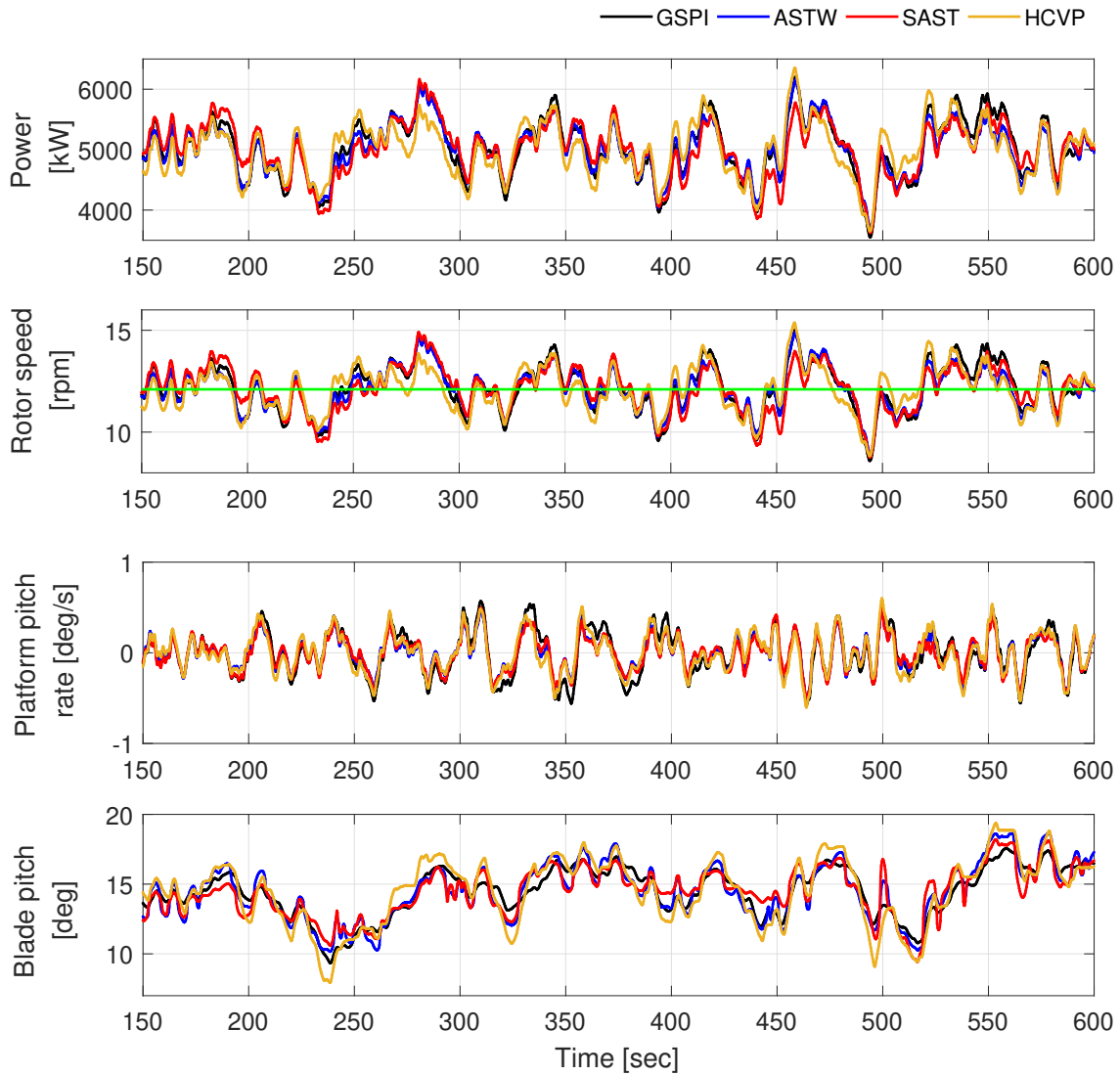


Figure 2.10 – **Scenario 3.** Main variables of the FWT versus time (*sec*) respectively, obtained by GSPI (black), ASTW (blue), SAST (red) and HCVP (yellow). The green line in the second sub-figure indicates the rated rotor speed Ω_{r0} (12.1 *rpm*).

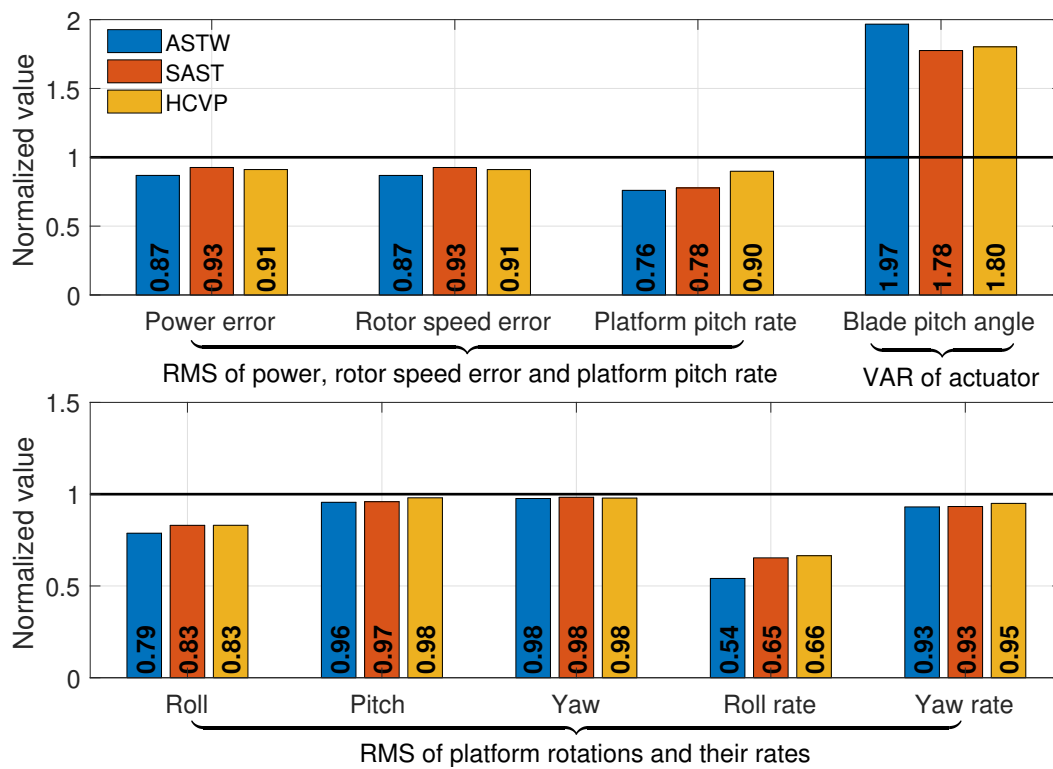


Figure 2.11 – **Scenario 3**. Normalized RMS/VAR values of performances indicators obtained by ASTW (blue), SAST (red) and HCVP (yellow) controllers.

comparing with GSPI: ASTW slightly reduces the tower base load and slightly increases the blade root flap-wise moment by +5%. SAST has almost no influence on the tower base and blade root load whereas HCVP allows a reduction of the tower base side-to-side load by -8% but induces an increase of the blade root flap-wise moment by +12%. Figure 2.13 shows the normalized DEL of the fair-lead force (FF) and anchor force (AF) of the 3 mooring lines. SAST and HCVP controllers decrease FF and AF loads of the mooring lines about 10%. However, ASTW increases these loads about 10%.

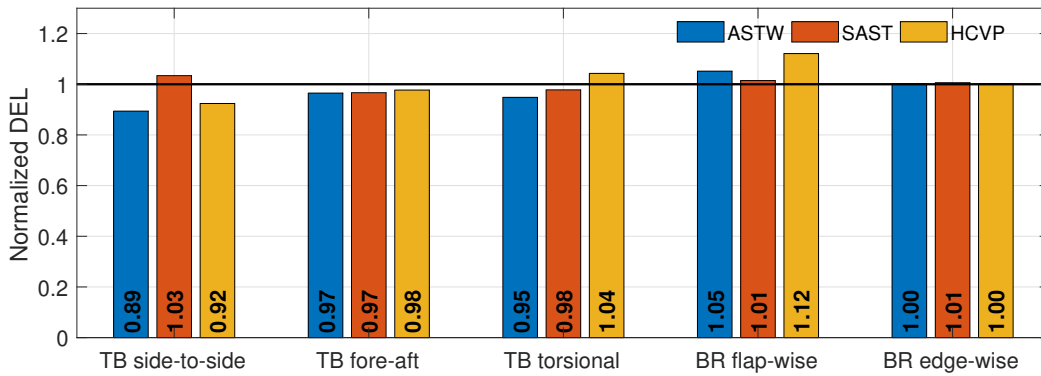


Figure 2.12 – **Scenario 3.** Normalized DEL values of TB and BR loads obtained by ASTW (blue), SAST (red) and HCVP (yellow) controllers.

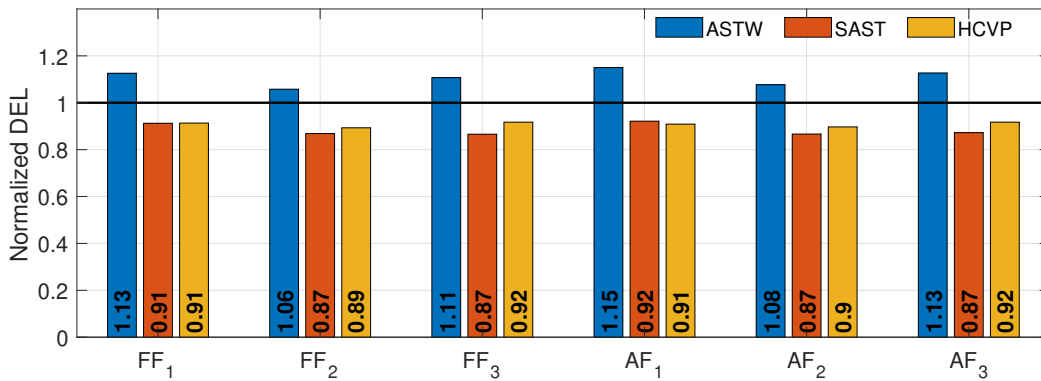


Figure 2.13 – **Scenario 3.** Normalized DEL values of mooring line loads obtained by ASTW (blue), SAST (red) and HCVP (yellow) controllers.

Recall that the ASTW, SAST and HCVP controllers are based on gain/parameter adaptation algorithms. Figure 2.14 shows ASTW gain k_1 (top), SAST gain L (middle) and adaptive exponent $\bar{\alpha}$ (bottom) for HCVP. The variation of the gains/parameter illustrate their dynamical adaptation versus the wind and wave perturbations; it clearly shows that

- for ASTW and SAST control, a time-varying gain offers a good opportunity to limit the gain versus the operating conditions;
- for HCVP control, the parameter $\bar{\alpha}$ that varies from $[0, 1]$ allows to reduce the chattering of the controller. Notice that the average value of $\bar{\alpha}$ for $t \in [100, 600]$ is 0.07.

Notice from Figure 2.15 that, after a transient time and for the three controllers, the sliding variables are converging towards a vicinity of 0.

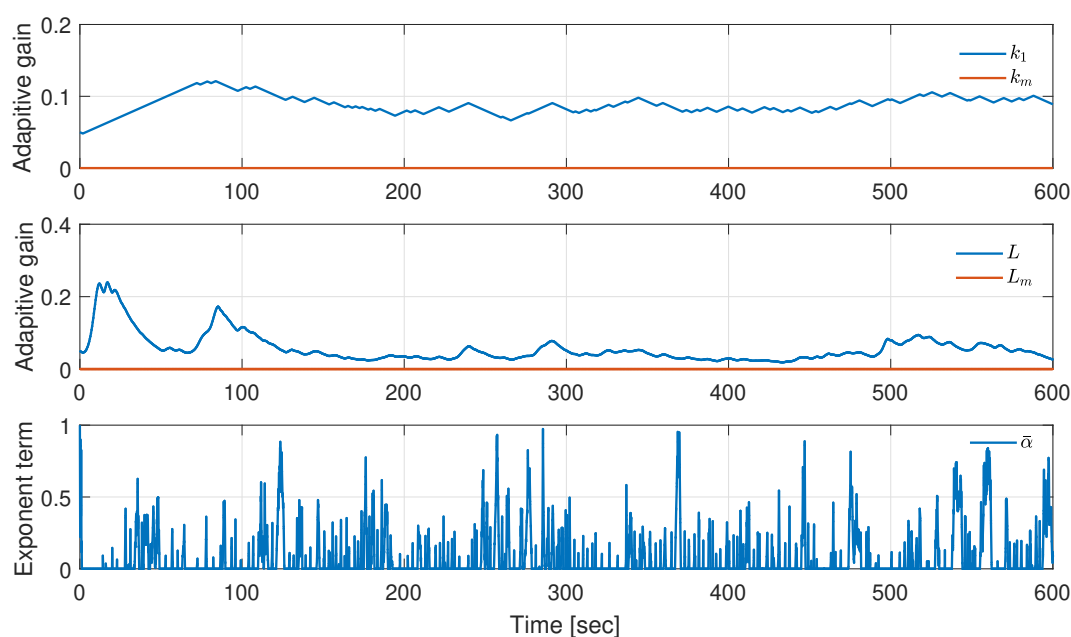


Figure 2.14 – **Scenario 3. Top.** ASTW controller gain k_1 (blue) and minimum value k_m (red) versus time (*sec*). **Middle.** SAST controller gain L (blue) and constant value L_m (red) versus time (*sec*). **Bottom.** HCVP exponent term $\bar{\alpha}$ versus time (*sec*).

Table 2.6 summarizes the performances information of the 4 controllers. It appears that SAST, with a very reduced number of parameters, allows to get among the best accuracy and the most reduced fatigue loads, with reasonable oscillations of blade pitch angle.

2.7 Conclusions

In this chapter, adaptive high order sliding mode control is applied to the FWT based on the collective blade pitch control. First, the formalization of the problem and the control objectives of the FWT are discussed: regulation of the rotor speed at its rated value (assuming that the generator

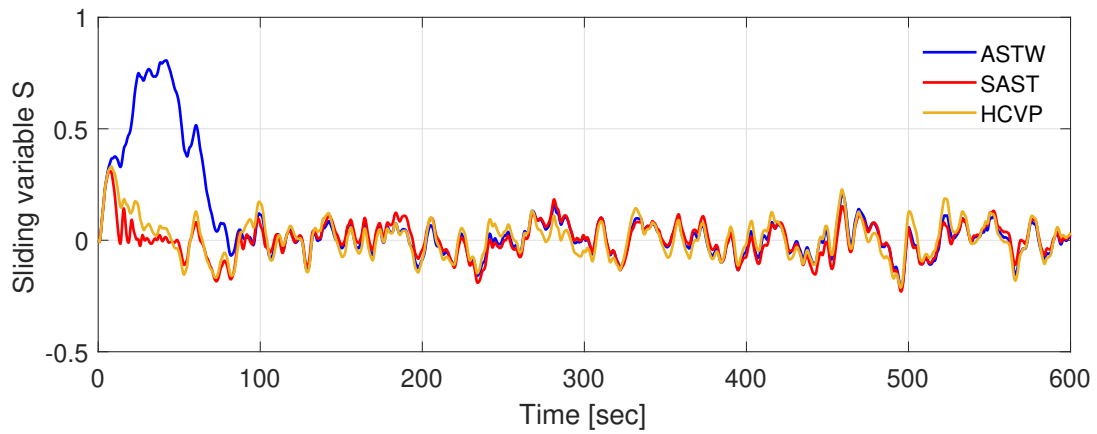


Figure 2.15 – **Scenario 3.** Sliding variable S versus time (sec) of ASTW (blue), SAST (red) and HCVP (yellow) controllers.

Table 2.6 – Performances information of the 4 controllers.

Control algorithm	Number of parameters	Accuracy of objectives	Actuator oscillation	Fatigue loads
GSPI	- - -	-	+ +	-
ASTW	+ +	+ +	- -	-
SAST	+ + +	+ +	- -	+
HCVP	+	+	- -	+

torque is fixed) and reduction of the platform pitch motion by using CBP control. Then, high order sliding mode control laws with different adaptation algorithms are recalled, including the adaptive super-twisting (ASTW) (Yuri Shtessel, Taleb, and Plestan 2012) and a recent developed homogeneity based controller with varying exponent parameter (HCVP) (Tahoumi, Plestan, et al. 2019). Meanwhile, a simplified adaptive super-twisting (SAST) algorithm with very few tuning parameters (only 2 parameters are must be tuned) is proposed. All of those algorithms are implemented to FWT in the FAST/SIMULINK environment and the performances are compared with the GSPI (J. Jonkman 2008a) control in different scenarios. Finally, the simulation results show that the adaptive control algorithms allow to successfully control the floating wind turbines in Region III with very reduced parameter tuning and knowledge of system modeling and have globally better performances than standard GSPI. Moreover, it appears that the proposed SAST control, with much less tuning parameters than ASTW and SAST, gives globally the best performances.